Effects of projectile resonances on the total, Coulomb, and nuclear breakup cross sections in the ^{6}Li + ^{152}Sm reaction

B. Mukeru* and M. L. Lekala†
Department of Physics, University of South Africa, South Africa
(Received 17 May 2016; published 2 August 2016)

In this paper we analyze the effects of the projectile resonances on the total, Coulomb, and nuclear breakup cross sections as well as on the Coulomb-nuclear interferences at different arbitrary incident energies. It is found that these resonances have non-negligible effects on the total, Coulomb, and nuclear breakup cross sections. Qualitatively, they have no effects on the constructiveness or destructiveness of the Coulomb-nuclear interferences. Quantitatively, we obtained that these resonances increase by 7.38%, 7.58%, and 20.30% the integrated total, Coulomb, and nuclear breakup cross sections, respectively at $E_{\rm lab} = 35$ MeV. This shows that the nuclear breakup cross sections are more affected by the effects of the projectile resonances than their total and Coulomb breakup counterparts. We also obtain that the effects of the resonances on the total, Coulomb, and nuclear breakup cross sections decrease as the incident energy increases.

DOI: 10.1103/PhysRevC.94.024602

I. INTRODUCTION

The study of nuclear reactions involving weakly bound projectiles on a variety of target masses has significantly advanced over the past decades, both experimentally and theoretically [1–10]. Being weakly bound, these nuclei can easily break into fragments, once in contact with a target or when going through the Coulomb field of a heavy target, making the breakup reactions a promising tool to study the structure of such nuclei. Some of the well-known results as far as the breakup reactions are concerned are strong bound-continuum and continuum-continuum couplings, rendering continuum states to play a rather important role in the breakup process [11–13]. These couplings can be of two kinds, resonant couplings and nonresonant couplings, depending on whether the coupled continuum states contain resonances or do not. This leads to two types of breakups: resonant and nonresonant breakups [14–18].

Although a lot of efforts have been made to understand the effects of the continuum-continuum couplings on other reaction channels, like elastic scattering and fusion, the effects of the projectile resonances (or resonant couplings) on breakup observables like breakup cross sections (total, Coulomb, and nuclear) is not fully established. In the Continuum-discretized coupled-channels (CDCC) method [19,20] (widely used to analyze breakup reactions, and which we also use in this paper), the inclusion of the resonant continuum states in the coupling matrix elements is not straightforward, in the sense that the discretization of resonant bins is more complex than the discretization of nonresonant bins. The former require finer bin widths, which in turn increase substantially the size of the coupling matrix elements and therefore increase the computational complexities. It is therefore crucial to assess the importance of the projectile resonances, because their exclusion when not important would result in a significant reduction of the computational load. It is equally important to verify to which extend the projectile resonances affect the Coulomb-nuclear interferences, which have been proven to play a key role in the breakup process [7,21,22].

The resonant and nonresonant breakups of ^{6}Li on various targets have been investigated in Refs. [14–18,23–25]. The authors in Refs. [23–25], have investigated the effects of the ^{6}Li resonances on the elastic scattering cross sections in the ^{6}Li + ^{28}Si, ^{58}Ni, ^{64}Zn, ^{144}Sm reactions, for incident energies below and around the Coulomb barrier have been analyzed. It was found in Ref. [23], that the exclusion of the resonances has small effects on the elastic-scattering cross sections for the two reactions. On the other hand, in Refs. [24,25], pronounced effects of the resonances were observed at backward angles. In light of these results, one may wonder whether the resonance effects on the elastic-scattering cross sections are target-mass or incident-energy dependent. Moreover, it is interesting to investigate whether these conclusions can also apply to other reaction channels, like breakup and fusion cross sections, for example.

In this paper, we study the qualitative and quantitative effects of the projectile resonances on the total, Coulomb, and nuclear breakup cross sections as well as on the Coulomb-nuclear interferences in the ^{6}Li + ^{152}Sm breakup reaction for a range of incident energies above the Coulomb barrier. We aim first to check whether the conclusions of Refs. [23–25] can be extended to breakup cross sections. Second, we will analyze the dependence of these effects on the incident energy. The results will shed more light on the role of the ^{6}Li resonances in the dynamics of the reactions induced by this nucleus. The reaction under study has already been analyzed in Ref. [26], to investigate the role of the projectile breakup on the fusion cross sections.

II. FORMALISM OF THE THREE-BODY CONTINUUM-DISCRETIZED COUPLED CHANNELS

The projectile ^{6}Li is considered as a cluster of alpha particle and deuteron (^{6}Li $\rightarrow \alpha + d$). Therefore, its interaction with an

*bmukeru@gmail.com
†lekalml@unisa.ac.za

inert target is regarded as a three-body system. The projectile internal Hamiltonian reads

$$h_{\alpha d} = -\frac{\hbar^2}{2\mu_{\alpha d}}\frac{d^2}{dr^2} + V_{\alpha d}(\mathbf{r}), \tag{1}$$

where $\mu_{\alpha d}$ is the projectile reduced mass and $V_{\alpha d}(\mathbf{r})$ the cluster interacting potential. The cluster's spin is that of a deuteron since the spin of the alpha particle is zero. Therefore, the bound and continuum (scattering and resonant) states of the projectile, which are eigenstates of the Hamiltonian $h_{\alpha d}$, are defined as

$$\Phi^m_\beta(\mathbf{r}) = \frac{1}{r}\phi^j_{k\ell}(r)\big[Y^{m_\ell}_\ell(\hat{\mathbf{r}}) \otimes X^{m_s}_s\big]_{jm}, \tag{2}$$

where $\beta = (k,\ell,s,j)$ represents the relevant quantum numbers describing the states of the projectile, and $X^{m_s}_s$ stands for the total internal wave function of deuteron. The continuum states $\phi^j_{k\ell}(r)$ of Eq. (2) are normalized according to

$$\phi^j_{k\ell}(r\to\infty) \to F_\ell(kr)\cos\delta_{\ell j}(k) + G_\ell(kr)\sin\delta_{\ell j}(k), \tag{3}$$

where F_ℓ and G_ℓ are Coulomb functions [27], and $\delta_{\ell j}(k)$ is the nuclear phase shift.

The continuum wave functions $\phi^j_{k\ell}(r)$ are not square integrable. However, in the CDCC framework, and adopting the binning method [19,28,29], these wave functions are sliced into bins of widths $\Delta k_i = k_i - k_{i-1}$, averaged over the relative momentum k. With this method, one obtains discretized continuum wave functions, which are square integrable and defined as [29]

$$\varphi_\beta(r) = \sqrt{\frac{2}{\pi W_\beta}}\int_{k_{i-1}}^{k_i} \mathrm{g}_\beta(k)\phi^j_{k\ell}(k)dk, \quad i = 1,2,\ldots,N_b, \tag{4}$$

where $\mathrm{g}_\beta(k)$ is some weight function and $W_\beta = \int_{k_{i-1}}^{k_i}|\mathrm{g}_\beta(k)|^2dk$ is the normalization coefficient. The subscript β becomes $\beta = (i,\ell,s,j)$, where $\beta_0 = (0,\ell_0,s,j_0)$ refers to the ground state. The bin wave functions (4) are associated with the following bin energies:

$$\varepsilon_\beta = \frac{\hbar^2}{2\mu_{\alpha d}W_\beta}\int_{k_{i-1}}^{k_i} k^2|\mathrm{g}_\beta(k)|^2dk. \tag{5}$$

The definition of the weight function $\mathrm{g}_\beta(k)$ depends on the bin states. For non-S-wave nonresonant bins, $\mathrm{g}_\beta(k)$ is commonly set to $\mathrm{g}_\beta(k) = 1$. In this case, Eq. (5) becomes

$$\varepsilon_\beta = \frac{\hbar^2}{2\mu_{\alpha d}}\frac{1}{3}\big(k_i^2 + k_ik_{i-1} + k_{i-1}^2\big). \tag{6}$$

For S-wave bins, it is convenient to use $g_\beta(k) = k$, because this stabilizes the extraction of the three-body transition amplitude [28,29], in which case $W_\beta = \frac{\Delta k_i}{3}(k_i^2 + k_ik_{i-1} + k_{i-1}^2)$, and

$$\varepsilon_\beta = \frac{\hbar^2\hat{k}_i}{2\mu_{\alpha d}}, \tag{7}$$

where

$$\hat{k}_i = \frac{3}{5}\left(\frac{k_i^4 + k_i^3k_{i-1} + k_i^2k_{i-1}^2 + k_ik_{i-1}^2 + k_{i-1}^4}{k_i^2 + k_ik_{i-1} + k_{i-1}^2}\right). \tag{8}$$

For resonant bins on the other hand, we follow Ref. [30] and define

$$\mathrm{g}_\beta = \left|\frac{\frac{i}{2}\Gamma}{\varepsilon(k) - \varepsilon_r + \frac{i}{2}\Gamma}\right|, \tag{9}$$

where $\varepsilon(k)$ is a continuous intrinsic energy of α-d, and ε_r and Γ are the resonance energy and width, respectively. The physics behind the discretization in Eq. (4) is explained more in Ref. [31].

The construction of the bin wave functions allows one to expand three-body CDCC wave function as follows:

$$\Psi^{\mathrm{CDCC}}_{JM}(\mathbf{r},\mathbf{R}) = \frac{1}{R}\sum_{\beta,L}\chi^{LJ}_\beta(R)\mathcal{F}_{\beta L}(\mathbf{r},\hat{R}), \tag{10}$$

where the channel wave function $\mathcal{F}_{\beta L}(\mathbf{r},\hat{R})$ is given by

$$\mathcal{F}_{\beta L}(\mathbf{r},\hat{R}) = \big[i^L\hat{\Phi}^m_\beta(\mathbf{r}) \otimes Y^{M_L}_L(\hat{R})\big]_{JM}, \tag{11}$$

with

$$\hat{\Phi}^m_\beta(\mathbf{r}) = \frac{1}{r}\varphi_\beta(r)\big[i^\ell Y^{m_\ell}_\ell(\hat{\mathbf{r}}) \otimes X^{m_s}_s\big]_{jm}, \tag{12}$$

where $\varphi_\beta(r)$ is given by Eq. (4).

The CDCC wave function (10) is an eigenstate of the three-body Hamiltonian

$$H_{3\mathrm{B}} = T_R + h_{\alpha d} + V_{\alpha t}\big(\mathbf{R} + \tfrac{2}{6}\mathbf{r}\big) + V_{dt}\big(\mathbf{R} - \tfrac{4}{6}\mathbf{r}\big), \tag{13}$$

where

$$T_R = -\frac{\hbar^2}{\mu_{pt}}\frac{d^2}{dR^2}, \tag{14}$$

with μ_{pt} being the projectile-target reduced mass. In Eq. (13), $V_{\alpha t}$ and V_{dt} are the alpha-target and deuteron-target potentials, respectively. The substitution of the expansion (10) into the three-body Schrödinger equation involving the Hamiltonian (13) leads to a set of coupled equations for the coefficients $\chi^{LJ}_\beta(R)$, reading

$$\begin{aligned}&\big[\mathcal{T}_R + U^{LJ}_{\beta\beta}(R) + \varepsilon_\beta - E\big]\chi^{LJ}_\beta(R)\\ &\quad - \sum_{\beta\neq\beta'} i^{L-L'}U^{LL'J}_{\beta\beta'}(R)\chi^{L'J}_{\beta'}(R) = 0,\end{aligned} \tag{15}$$

where

$$\mathcal{T}_R = -\frac{\hbar^2}{2\mu_{pt}}\left(\frac{d^2}{dR^2} - \frac{L(L+1)}{R^2}\right), \tag{16}$$

and $U^{LJ}_{\beta\beta}(R)$, $U^{LL'J}_{\beta\beta'}(R)$ are respectively the diagonal and off-diagonal potential matrix elements given by

$$U^{LL'J}_{\beta\beta'}(R) = \langle\mathcal{F}_{\beta L}(\mathbf{r},\hat{R})|V_{pt}|\mathcal{F}_{\beta' L'}(\mathbf{r},\hat{R})\rangle, \tag{17}$$

where $V_{pt} = V_{\alpha t}(R_{\alpha t}) + V_{dt}(R_{dt})$, with

$$\begin{aligned}R^2_{\alpha t} &= R^2 + \tfrac{1}{9}r^2 + \tfrac{2}{3}Rrz,\\ R^2_{dt} &= R^2 + \tfrac{4}{9}r^2 - \tfrac{4}{3}Rrz,\end{aligned} \tag{18}$$

with z being the cosine of the angle between vectors $\mathbf{r}$ and $\mathbf{R}$. After a numerical evaluation of the potential matrix elements,

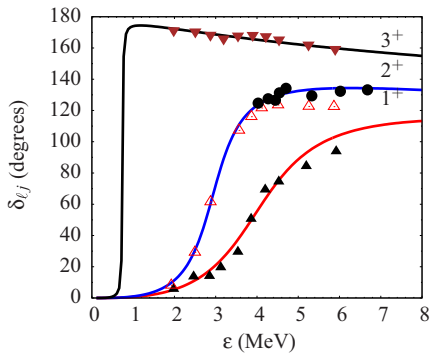

FIG. 1. Resonance structure in the $\ell = 2$ ($j^\pi = 1^+,\ 2^+,\ 3^+$) continuum states. The filled and open triangle experimental data points are taken from Ref. [34], and the solid circular data points are from Ref. [35].

the coupled equations (15) are solved subject to the usual boundary conditions at $R \to \infty$,

$$\chi_\beta^{LJ}(R) \to \frac{i}{2}[H_\beta^-(K_\beta R)\delta_{\beta\beta'} - H_\beta^+(K_\beta R)S_{\beta\beta'}(K_\beta)], \qquad (19)$$

where $H_\beta^\pm(K_\beta R)$ are Coulomb Hankel functions [27], and $S_{\beta\beta'}(K_\beta)$ is the breakup S matrix, with $K_\beta = [2\mu_{pt}(E + \varepsilon_\beta)/\hbar^2]^{1/2}$, from which the breakup observables are obtained as described; for example, in Ref. [28].

III. DETAILS OF THE CALCULATIONS

The projectile ground-state separation energy is $\varepsilon_0 = -1.47$ MeV, with quantum numbers $n = 2$, $\ell = 0$, and $j^\pi = 1^+$ [32]. Its continuum states exhibit three resonances in the $\ell = 2$ ($j^\pi = 1^+,2^+,3^+$) partial waves, with experimental energies and widths, $(\varepsilon_{1^+};\Gamma_{1^+}) = (4.18\ \text{MeV}; 1.5\ \text{MeV}), (\varepsilon_{2^+};\Gamma_{2^+}) = (2.84\ \text{MeV}; 1.7\ \text{MeV})$ and $(\varepsilon_{3^+};\Gamma_{3^+}) = (0.716\ \text{MeV}; 0.024\ \text{MeV})$, respectively [33]. The parameters of the Woods–Saxon $V_{\alpha d}(r)$ potential used to generate the projectile ground state are $V_0 = 78.46$ MeV, $r_0 = 1.15$ fm, $a_0 = 0.7$ fm. To reproduce the three resonances, the depth V_0 is adjusted to $V_0 = 80.0$ MeV and a spin-orbit term of $V_{\text{SO}} = 2.5\ \text{MeV fm}^2$ is added. All these parameters are taken from Ref. [33], which we check by plotting in Fig. 1 the phase shifts against the excitation energies, where a fair agreement between the experimental resonances and our calculations is observed, especially for $j^\pi = 3^+$. The other potential parameters needed in the calculations are those of $V_{\alpha t}$ and V_{dt} potentials, which are listed in Table I. The CDCC model space parameters (related to the bin discretization and numerical integration) are given in Table II. We verified that these parameters are enough to guarantee the convergence of the results.

TABLE I. Alpha-target and deuteron-target optical potential parameters used in the calculations. $R_i = r_i A_T^{1/3}$, where A_T is the target mass.

$\alpha/d + t$	V (MeV)	W (MeV)	r_R (fm)	r_I (fm)	a_R (fm)	a_I (fm)	r_C (fm)	Ref.
$\alpha + t$	60.50	18.72	1.436	1.343	0.607	0.735	1.404	[36]
$d + t$	91.48	24.81	1.150	1.344	0.925	0.579	1.250	[37]

TABLE II. CDCC model space parameters required for convergence.

$\ell_{\max}$ ($\hbar$)	$\lambda_{\max}$	$\varepsilon_{\max}$ (MeV)	$r_{\max}$ (fm)	Δr (fm)	$L_{\max}$ ($\hbar$)	$R_{\max}$ (fm)	ΔR (fm)
3	4	8	180	0.1	1000	600	0.06

The interval $[0,\varepsilon_{\max}]$ is discretized into bin states of widths $\Delta\varepsilon = 0.5$ MeV for the $\ell = 0$ ($j^\pi = 1^+$) and $\ell = 1$ ($j^\pi = 0^-,1^-,2^-$) partial waves, whereas for the $\ell = 3$ ($j^\pi = 2^-,3^-,4^-$) partial wave we adopt $\Delta\varepsilon = 1$ MeV. For resonant bins where finer widths are required, we resort to the discretization of Ref. [33], where for the $j^\pi = 3^+$ resonance, $\Delta\varepsilon = 0.1299$ MeV below, $\Delta\varepsilon = 0.5208$ MeV above, and $\Delta\varepsilon = 0.1$ MeV inside the resonance. For the $j^\pi = 1^+,2^+$ resonances, $\Delta\varepsilon = 0.4$ MeV below and inside and $\Delta\varepsilon = 0.5$ MeV above these resonances. In order to analyze the effects of the resonances on the total, Coulomb, and nuclear breakup cross sections, we remove the resonant couplings in the potential matrix elements by treating the $\ell = 2$ partial wave as any other nonresonant partial wave, and it is discretized similar to the $\ell = 0,1$ partial waves, i.e., $\Delta\varepsilon = 0.5$ MeV, for all $j^\pi = 1^+$, 2^+, and 3^+ partial waves and the resulting bins are normalized accordingly. Although this procedure might not completely remove the effect of resonances, we believe that this work will shed more light into the effects of the resonances on the breakup cross sections. Our numerical calculations are performed by using FRESCO [38].

IV. RESULTS AND DISCUSSION

A. Differential total, Coulomb, and nuclear breakup cross sections

We start by considering effects of the resonances on the differential total, Coulomb, and nuclear breakup cross sections. The results obtained for the total breakup are presented in Fig. 2 for $E_{\text{lab}} = 35$ MeV, 45 MeV and those for $E_{\text{lab}} = 50$ MeV, 60 MeV in Fig. 3. Qualitatively, looking at Fig. 2(a), one observes that, in the presence of resonances (resonant breakup), the breakup cross section (full line) is slightly dominant at backward angles, whereas in the absence of resonances (nonresonant breakup), the breakup cross section (dotted line) is dominant at $10^\circ \leqslant \theta \leqslant 40^\circ$ and peaks around 30°, while at $\theta \leqslant 10^\circ$, the two breakup cross sections are hardly distinguishable. A similar trend is observed in Fig. 2(b), although here the peak around 15° is less pronounced. Considering the results obtained for $E_{\text{lab}} = 50$ MeV, 60 MeV [Figs. 3(a) and 3(b)], it is noticed that one can still draw similar conclusions as for $E_{\text{lab}} = 35$ MeV, 45 MeV, but the breakup cross sections are less affected by the resonances. We can conclude that the effects of the resonances are to slightly decrease (increase) the total breakup cross section at forward (backward) angles. Similar conclusions were reached

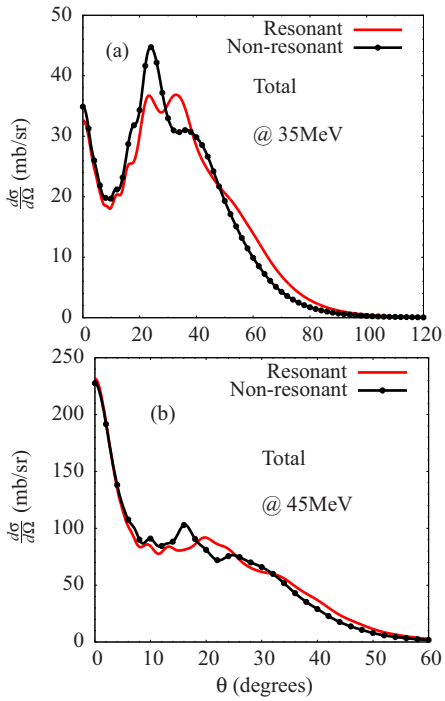

FIG. 2. Resonant and nonresonant differential total breakup cross sections at (a) $E_{\text{lab}} = 35$ MeV and (b) $E_{\text{lab}} = 45$ MeV.

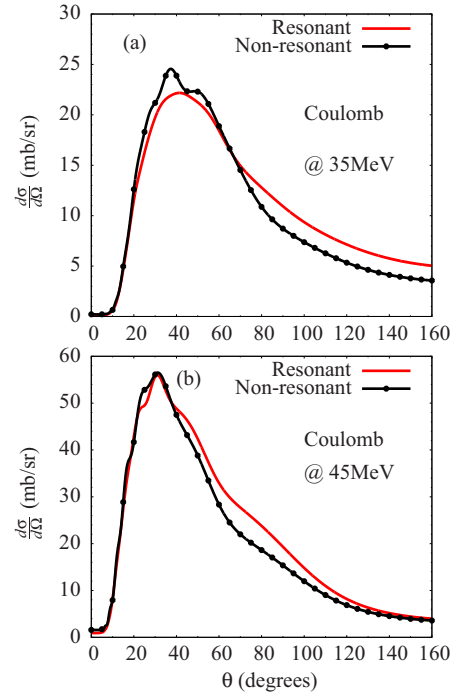

FIG. 4. Resonant and nonresonant differential Coulomb breakup cross sections at (a) $E_{\text{lab}} = 35$ MeV and (b) $E_{\text{lab}} = 45$ MeV.

in Refs. [23,24], on the elastic scattering cross sections and on the breakup cross sections in Ref. [15] (see Fig. 2 of this reference). A further look at Figs. 3(a) and 3(b) shows clearly that the resonance effects decrease with the increase of the incident energy.

The Coulomb breakup cross sections are reported in Figs. 4 and 5. Both figures show that the resonances increase

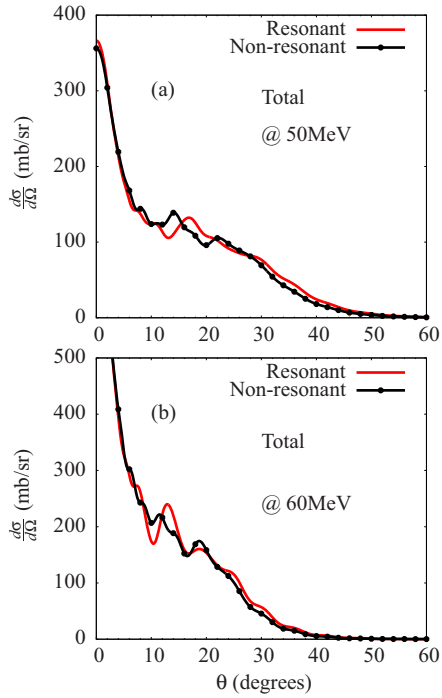

FIG. 3. Resonant and nonresonant differential total breakup cross sections at (a) $E_{\text{lab}} = 50$ MeV and (b) $E_{\text{lab}} = 60$ MeV.

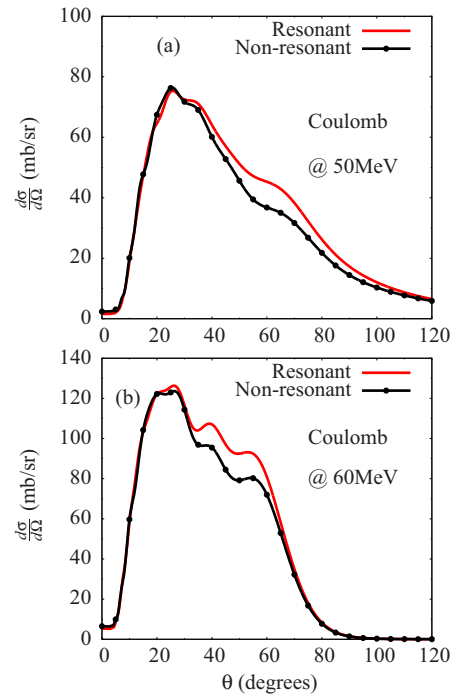

FIG. 5. Resonant and nonresonant differential Coulomb breakup cross sections at (a) $E_{\text{lab}} = 50$ MeV, (b) $E_{\text{lab}} = 60$ MeV.

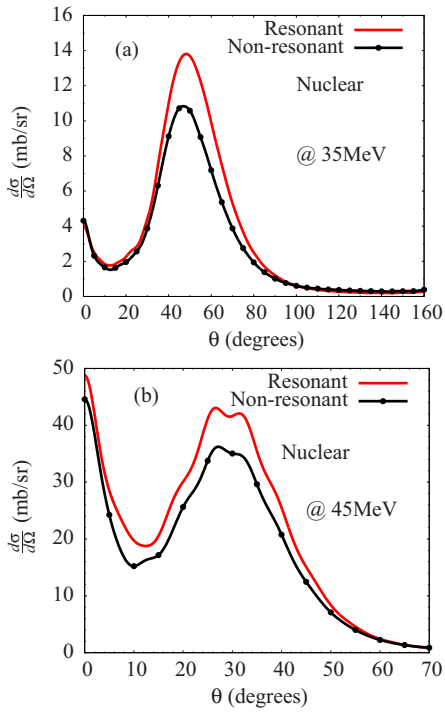

FIG. 6. Resonant and nonresonant differential nuclear breakup cross sections at (a) $E_{\rm lab} = 35$ MeV, (b) $E_{\rm lab} = 35$ MeV.

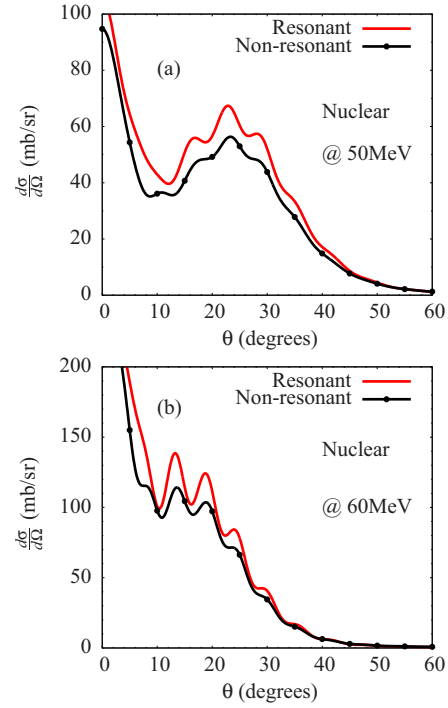

FIG. 7. Resonant and nonresonant differential nuclear breakup cross sections at (a) $E_{\rm lab} = 50$ MeV, (b) $E_{\rm lab} = 50$ MeV.

the breakup cross sections at backward angles, and as the incident energy increases, their effects are negligible at forward angles ($\theta \leqslant 40^\circ$ for $E_{\rm lab} = 45$ MeV, and $\theta \leqslant 30^\circ$ for $E_{\rm lab} = 50,\ 60$ MeV). Looking at the total and Coulomb breakup results, we can conclude that the projectile resonances affect qualitatively both the total and Coulomb breakup cross sections in a similar way.

The nuclear breakup cross sections are presented in Figs. 6 and 7. It is seen that, for $E_{\rm lab} \geqslant 45$ MeV, the resonant nuclear breakup cross sections are dominant at forward angles. Compared with the total and Coulomb breakup cross sections, one notices that the nuclear breakup cross sections are more affected by the resonances, especially at forward angles.

B. Coulomb-nuclear interferences

The above results obtained for the total, Coulomb, and nuclear differential breakup cross sections imply that the projectile resonances would have non-negligible effects on the Coulomb-nuclear interferences. However, these results do not provide enough information on the constructiveness or destructiveness of these interferences. In this section, we focus on the qualitative effects of the resonances on the differential Coulomb-nuclear interferences. To this end, we first define the differential Coulomb-nuclear interferences of the angular distributions as

$$\frac{d\sigma^{\rm int}}{d\Omega} = \frac{d\sigma^{\rm tot}}{d\Omega} - \left(\frac{d\sigma^{\rm coul}}{d\Omega} + \frac{d\sigma^{\rm nucl}}{d\Omega}\right), \qquad (20)$$

which are constructive where $\frac{d\sigma^{\rm int}}{d\Omega} \geqslant 0$ and destructive where $\frac{d\sigma^{\rm int}}{d\Omega} \leqslant 1$. These interferences are plotted in Figs. 8 and 9 for $E_{\rm lab} = 35,\ 45$ MeV and $E_{\rm lab} = 50,\ 60$ MeV, respectively. The two figures show that, at forward angles ($\theta \leqslant 30^\circ$ for $E_{\rm lab} = 35$ MeV, $\theta \leqslant 20^\circ$ for $E_{\rm lab} = 45$ MeV, $\theta \leqslant 10^\circ$ for $E_{\rm lab} = 50$ MeV and $E_{\rm lab} = 60$ MeV) and in the presence

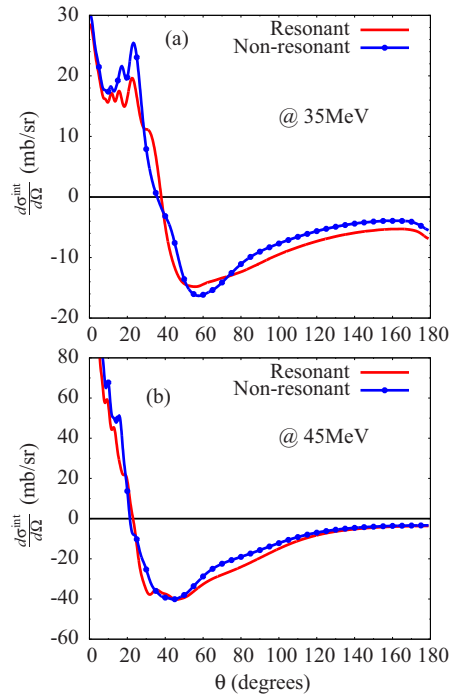

FIG. 8. Resonant and nonresonant Coulomb-nuclear interferences for (a) $E_{\rm lab} = 35$ MeV and (b) $E_{\rm lab} = 45$ MeV.

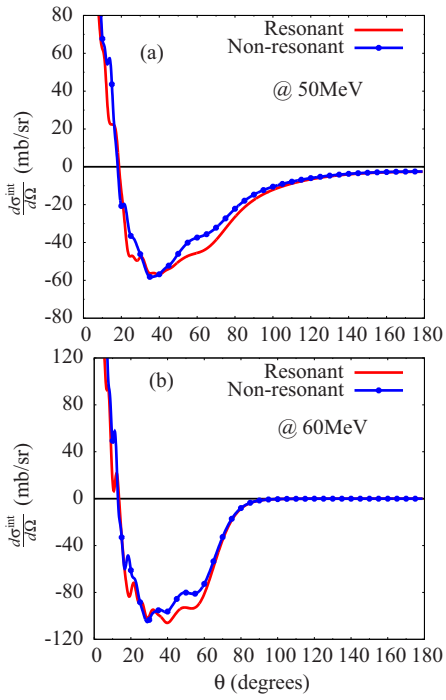

FIG. 9. Resonant and nonresonant Coulomb-nuclear interferences for (a) $E_{lab} = 50$ MeV and (b) $E_{lab} = 60$ MeV.

of the resonances, the Coulomb-nuclear interferences are exclusively constructive. At backward angles, on the other hand, they are destructive. It is seen that this destructiveness decreases as the incident energy increases, such that for $E_{lab} = 60$ MeV, $\frac{d\sigma^{int}}{d\Omega} \simeq 0$ at $\theta \geqslant 80^{\circ}$. It is noticed that the absence of the resonances does not affect the constructiveness or destructiveness of the Coulomb-nuclear interferences. One concludes that the resonances do not have any qualitative effects on the Coulomb-nuclear interferences. However, we notice clear quantitative effects, which are discussed in the next section.

C. Angular-integrated total, Coulomb, and nuclear breakup cross sections

To gain more insight into this study, we analyze the quantitative effects of these resonances on the total, Coulomb and nuclear breakup cross sections, as well as on the Coulomb-nuclear interferences. To this end, the differential breakup cross sections of the angular distributions are numerically integrated by using

$$\sigma^{x} = 2\pi \int_{0}^{\theta^{max}} \frac{d\sigma_{x}}{d\theta} \sin\theta d\theta, \quad x \equiv \text{tot, coul, nucl}, \qquad (21)$$

after the use of $d\Omega = 2\pi \sin\theta d\theta$. The angular-integrated breakup cross sections for the four incident energies are summarized in Table III. In this table, σ_{R}^{x} and σ_{NR}^{x} represent the breakup cross section with and without resonances, respectively and σ^{int} stands for the Coulomb-nuclear interferences. The quantities Δ_{tot}, Δ_{coul}, Δ_{nucl}, and Δ_{int} (in percentage), defined as $\Delta_{x} = (1 - \sigma_{NR}^{x}/\sigma_{R}^{x}) \times 100\%$, are used to estimate the effects of the projectile resonances on the total, Coulomb, and nuclear breakup cross sections and on the Coulomb-nuclear interferences. Starting with the breakup cross sections, the results show that, for the total and nuclear breakups, the contributions of the resonances to the integrated breakup cross sections decrease as the incident energy increases. For the total breakup, we observe that the breakup cross sections are increased by 7.38% owing to the resonances for $E_{lab} = 35$ MeV and by less than 7% for the other incident energies. For the nuclear breakup, on the other hand, it can be seen that the resonances increase the breakup cross sections by 20.30%, for $E_{lab} = 35$ MeV and by less than 16% for the other incident energies. For the Coulomb breakup, however, we notice that the breakup cross sections are increased by 3.66% from $E_{lab} = 35$ MeV to $E_{lab} = 45$ MeV and decreased by 2.92% from $E_{lab} = 45$ MeV to $E_{lab} = 60$ MeV, and overall effects are less than 12%. These numbers show again that the effects of the projectile resonances are more pronounced on the nuclear breakup cross sections than on its total and Coulomb breakup counterparts, as already stated. Moreover, in light of these results, it can be predicted that, for higher incident energies, the effects of the resonances could be rather negligible on the three different breakup cross sections.

Finally, the results obtained for the Coulomb-nuclear interferences show that these interferences are exclusively destructive at all the incident energies, regardless of whether the resonances are included. This destructiveness is strengthened as the incident energy increases. This indicates again clearly that the resonances have no qualitative effects on the Coulomb-nuclear interferences, as already pointed out. Quantitatively, one can see that these interferences are increased from 13.82% to 15.25% from $E_{lab} = 35$ MeV to $E_{lab} = 45$ MeV, from which it drops to 10.16% for $E_{lab} = 60$ MeV. This is also an indication that higher incident energies would amount

TABLE III. Energy-integrated resonant and resonant total, Coulomb and nuclear breakup cross sections (in barns), as well as the Coulomb-nuclear interferences.

Energy	With resonances				Without resonances				Estimated resonances contributions			
	σ_{R}^{tot}	σ_{R}^{coul}	σ_{R}^{nucl}	σ_{R}^{int}	σ_{NR}^{tot}	σ_{NR}^{coul}	σ_{NR}^{nucl}	σ_{NR}^{int}	Δ_{tot}	Δ_{coul}	Δ_{nucl}	Δ_{int}
35 MeV	5.667	8.467	2.512	−5.312	5.249	7.825	2.002	−4.578	7.38%	7.58%	20.30%	13.82%
45 MeV	7.169	15.656	3.912	−12.399	6.696	13.896	3.308	−10.508	6.60%	11.24%	15.44%	15.25%
50 MeV	7.656	18.642	4.510	−15.496	7.176	16.698	3.895	−13.417	6.27%	10.43%	13.64%	13.42%
60 MeV	8.345	22.675	5.456	−19.786	7.862	20.788	4.849	−17.775	5.79%	8.32%	11.12%	10.16%

to negligible resonance effects on the Coulomb-nuclear interferences.

V. CONCLUSIONS

In this paper we investigate in detail the effects of the projectile resonances on the total, Coulomb, and nuclear breakup cross sections as well as on the Coulomb-nuclear interferences for the ^{6}Li + ^{152}Sm reaction at different incident energies. To achieve this, we removed the resonant bins from the coupling matrix by discretizing the $\ell = 2$ resonant partial wave as any other nonresonant partial wave and the bins were normalized accordingly. The results showed that the projectile resonances have non-negligible effects on the total, Coulomb, and nuclear breakup cross sections. The nuclear breakup cross sections are more affected by these resonances than the total and Coulomb breakup cross sections. Qualitatively, these resonances do not have any effects on the constructiveness or destructiveness of the Coulomb-nuclear interferences.

Quantitatively, we find that these resonances increase by 7.38%, 7.58%, and 20.30% the total, Coulomb, and nuclear integrated breakup cross sections, respectively for $E_{\rm lab} = 35$ MeV. For the same incident energy, the Coulomb-nuclear interferences are increased by 13.82% and remain exclusively destructive regardless of whether these resonances are included. It is also obtained that these effects decrease as the incident energy increases. We then conclude that, for higher energies, the resonance effects on the total, Coulomb, and nuclear breakup cross section, as well as on the Coulomb-nuclear interferences could be negligible.

ACKNOWLEDGMENTS

We are thankful to Professor I. J. Thompson for useful discussions, especially regarding FRESCO codes.

[1] I. Tanihata, H. Hamagaki, O. Hashimoto, Y. Shida, N. Yoshikawa, K. Sugimoto, O. Yamakawa, T. Kobayashi, and N. Takahashi, Measurements of Interaction Cross Section and Nuclear Radii in Light *p*-Shell Region, Phys. Rev. Lett. **55**, 2676 (1985).

[2] G. Baur, C. A. Bertulani, and H. Rebel, Coulomb dissociation as a source of information on radioactive capture processes of astrophysical interest, Nucl. Phys. A **458**, 188 (1986).

[3] I. Tanihata, H. Savajols, and R. Kanungo, Recent experimental progress in nuclear halo structure studies, Prog. Part. Nucl. Phys. **68**, 215 (2013).

[4] C. Beck *et al.*, Nuclear-barrier fusion of weakly bound ^{6}Li and ^{7}Li nuclei with ^{59}Co, Phys. Rev. C **67**, 054602 (2003).

[5] M. Dasgupta, P. R. S. Gomes, D. J. Hinde, S. B. Moraes, R. M. Anjos, A. C. Berriman, R. D. Butt, N. Carlin, J. Lubian, C. R. Morton, J. O. Newton, and A. Szanto de Toledo, Effect of breakup on fusion of ^{6}Li, ^{7}Li, and ^{9}Be on heavy nuclei, Phys. Rev. C **70**, 024606 (2004).

[6] B. Mukeru and M. L. Lekala, First-order and higher-order interferences in the ^{11}Be + ^{208}Pb and ^{15}C + ^{208}Pb reactions, Phys. Rev. C **91**, 064609 (2015).

[7] M. S. Hussein, R. Lichtenthaler, F. M. Nunes, and I. J. Thompson, Scaling and interference in the dissociation of halo nuclei, Phys. Lett. B **640**, 91 (2006).

[8] D. R. Otomar *et al.*, Nuclear and Coulomb breakup of weakly bound 6 Li nucleus with targets in the range from $A = 59$ to $A = 208$, Phys. Rev. C **87**, 014615 (2013).

[9] T. Nakamura *et al.*, Halo Structure of the Island of Inversion ^{31}Ne, Phys. Rev. Lett. **103**, 262501 (2009).

[10] T. Aumann and T. Nakamura, The electric dipole response of exotic nuclei, Phys. Scr. **T152**, 014012 (2013).

[11] A. Diaz-Torres and I. J. Thompson, Effect of continuum couplings in fusion of halo ^{11}Be on ^{208}Pb around the Coulomb barrier, Phys. Rev. C **65**, 024606 (2002).

[12] L. F. Canto, J. Lubian, P. R. S. Gomes, and M. S. Husse, Continuum-continuum couplings and polarization potentials for weakly bound systems, Phys. Rev. C **80**, 047601 (2009).

[13] B. Mukeru, M. L. Lekala, and A. S. Denikin, Role of the diagonal and off-diagonal continuum-continuum couplings in the breakup of ^{8}B and ^{19}C on ^{58}Ni and ^{208}Pb targets, Nucl. Phys. A **935**, 18 (2015).

[14] J. Kiener, H. J. Gils, H. Rebel, S. Zagromski, G. Gsottschneider, N. Heide, H. Jelitto, J. Wentz, and G. Baur, Measurements of the Coulomb dissociation cross sections of 156 MeV ^{6}Li projectiles at extremely low relative fragment energies of astrophysical interest, Phys. Rev. C **44**, 2195 (1991).

[15] N. Keeley and K. Rusek, The role of breakup in near-barrier energy ^{6}Li + ^{208}Pb scattering, Phys. Lett. B **375**, 9 (1996).

[16] H. Gemmeke, B. Deluigi, L. Lassen, and D. Scholz, Coulomb and nuclear excitation in the sequential breakup of ^{6}Li, Z. Phys. A: At. Nucl. (1975) **286**, 73 (1978).

[17] R. Shyam, G. Baur, and P. Banerjee, Projectile breakup by nuclear and coulomb fields and application to astrophysically relevant radioactive capture processes, Phys. Rev. C **44**, 915 (1991).

[18] Y. Hirabayashi and Y. Sukaragi, Evidence of Strong Nuclear Breakup Contribution to ^{6}Li $\rightarrow \alpha + d$ Breakup by ^{208}Pb, Phys. Rev. Lett. **69**, 1892 (1992).

[19] N. Austern *et al.*, Coupled-channels calculations for three-body models of deuteron-nucleus reactions, Phys. Rep. **154**, 125 (1987).

[20] Y. Iseri, M. Yahiro, and M. Kamimura, Coupled-channels approach to deuteron and ^{3}He breakup reactions, Prog. Theor. Phys. Suppl. **89**, 84 (1986).

[21] T. Tarutina and M. S. Hussein, Interference effects in the Coulomb dissociation of ^{15,17,19}C, Phys. Rev. C **70**, 034603 (2004).

[22] R. Chatterjee and R. Shyam, Coulomb-nuclear interference in the breakup of ^{11}Be, Phys. Rev. C **66**, 061601(R) (2002).

[23] A. Gomez Camacho, A. Diaz-Torres, P. R. S. Gomes, and J. Lubian, Effect of ^{6}Li resonances on near-barrier elastic scattering involving ^{28}Si and ^{58}Ni target nuclei, Phys. Rev. C **91**, 014607 (2015).

[24] J. P. Fernández-García *et al.*, Effects of coupling to breakup in the ^{6,7}Li + ^{64}Zn systems at near-barrier energies, Phys. Rev. C **92**, 054602 (2015).

[25] A. Gomes, A. Diaz-Torres, P. R. S. Gomes, and J. Lubian, Impact of ^{6}Li resonances on the near-barrier elastic scattering with ^{144}Sm, Phys. Rev. C **93**, 024604 (2016).

[26] P. K. Rath *et al.*, Fusion of ^{6}Li with ^{152}Sm: Role of the projectile breakup versus target deformation, Nucl. Phys. A **874**, 14 (2012).

[27] M. Abramowitz and I. A. Stegun, *Handbook of Mathematical Functions: With Formulas, Graphs, and Mathematical Tables* (National Bureau of Standards, Washington, DC, 1964).

[28] I. J. Thompson and F. M. Nunes, *Nuclear Reactions for Astrophysics* (Cambridge University Press, New York, 2009).

[29] J. A. Tostevin, F. M. Nunes, and I. J. Thompson, Calculations of three-body observables in ^{8}B breakup, Phys. Rev. C **63**, 024617 (2001).

[30] T. Matsumoto, T. Kamizato, K. Ogata, Y. Iseri, E. Hiyama, M. Kamimura, and M. Yahiro, New treatment of breakup continuum in the method of continuum discretized coupled channels, Phys. Rev. C **68**, 064607 (2003).

[31] C. A. Bertulani and L. F. Canto, Semiclassical calculation of Coulomb breakup of weakly-bound nuclei, Nucl. Phys. A **539**, 163 (1992).

[32] C. Beck, N. Keeley, and A. Diaz-Torres, Coupled-channel effects in elastic scattering and near-barrier fusion induced by weakly bound nuclei and exotic halo nuclei, Phys. Rev. C **75**, 054605 (2007).

[33] A. Diaz-Torres, I. J. Thompson, and C. Beck, How does breakup influence the total fusion of ^{6,7}Li at the Coulomb barrier?, Phys. Rev. C **68**, 044607 (2003).

[34] Y. Kikuchi, N. Kurihara, A. Wano, K. Katō, T. Myo, and Y. Takashina, Three-body model analysis of $\alpha + d$ elastic scattering and ^{2}H$(\alpha,\gamma)^{6}$Li reaction in complex-scaled solutions of the Lippman-Schwinger equation, Phys. Rev. C **84**, 064610 (2011).

[35] F. Hammache *et al.*, High-energy breakup of ^{6}Li as a tool to study Big Bang nucleosynthesis reaction ^{2}H$(\alpha,\gamma)^{6}$Li, Phys. Rev. C **82**, 065803 (2010).

[36] E. I. Obiajunwa, L. H. Rosier, and J. Van De Wiele, Elastic and inelastic scattering of proton and alpha particles from stable even samarium isotopes, Nucl. Phys. A **500**, 341 (1989).

[37] P. R. Christensen, A. Berinde, I. Neamu, and N. Scintei, Elastic scattering of 12 MeV deuterons on even rare-earth nuclei, Nucl. Phys. A **129**, 337 (1969).

[38] www.fresco.org.uk.